Organic & Biomolecular Chemistry

RSC Publishing

PAPER

[4 + 3] and [4 + 2] mechanisms of the Diels–Alder reactions of vinylboranes: an analysis of the electron charge density distribution†

Cite this: *Org. Biomol. Chem.*, 2013, **11**, 7953

Margarita M. Vallejos,*[a] Nélida M. Peruchena[b] and Silvina C. Pellegrinet*[a]

Received 31st July 2013,
Accepted 30th September 2013

DOI: 10.1039/c3ob41571f

www.rsc.org/obc

The Diels–Alder (DA) reactions of isoprene with vinylborane, dimethylvinylborane and dichlorovinylborane have been studied using density functional theory and the quantum theory of atoms in molecules. We evaluated the topological properties of the transition structures (TSs) and the evolution of such properties along the reaction paths. In accordance with previous studies, our results indicate that the *endo* TSs of the reaction with vinylborane present high [4 + 3] character, while the *exo* TSs and all the TSs of the reactions with dimethylvinylborane and dichlorovinylborane have [4 + 2] character. The higher charge concentration between the diene and the dienophile appears to account for the greater stabilization of the [4 + 3] TSs. The [4 + 3] structure turns into the [4 + 2] structure through a conflict mechanism in which the C_1 and B atoms compete to become attached to C_6. The C_6–B interaction, present from early steps of the reaction until beyond the TSs, plays a key role in facilitating the formation of the new σ-bonds. The [4 + 3] and [4 + 2] mechanisms for the DA reactions of boron-substituted dienophiles may be distinguished by analyzing the profile of the ellipticity at the C_1–C_6 bcp along the course of the reaction.

Introduction

The Diels–Alder (DA) reaction is one of the most important carbon–carbon bond-forming processes in organic synthesis.[1] The nature of the substituents on the diene and the dienophile is a key factor in controlling the reactivity and selectivity of the DA reaction.[2] In this sense, boron-activated alkenes have been demonstrated to be interesting dienophiles of high reactivity, regioselectivity, and *endo* stereoselectivity.[3] In addition, these versatile reagents constitute synthetic equivalents of diverse organic compounds such as enols, enamines and ketenes.[4–6] Singleton and others have extensively investigated the use of vinylboranes as DA dienophiles.[7–12] Based on *ab initio* calculations, Singleton proposed that in the DA reactions of butadiene with vinylborane and dimethylvinylborane *endo* transition structures (TSs) had nonclassical [4 + 3] character whereas *exo* TSs had classical [4 + 2] character.[13] Later, Goodman *et al.*[14] have theoretically studied the DA reactions of vinylboranes with substituted dienes to rationalize the origin of the regio- and stereoselectivity. The computed geometries of the *endo* TSs for the reactions of *trans*-piperylene and isoprene with vinylborane showed strong [4 + 3] character, although these led to the [4 + 2] cycloadducts. The strong C–B interactions predicted high *endo* stereoselectivity and anomalous *meta* regioselectivity. In contrast, in the TSs for dimethylvinylborane the C–B interaction is weaker as a consequence of the bulkiness of the alkyl groups attached to boron. Hence, these TSs adopt classical [4 + 2] character and the formation of *para* cycloadducts was favored for isoprene, while no regioselectivity was predicted for piperylene in accordance with experimental results. Further computational studies on the DA reactions of several dienes with dimethylvinylborane, vinyl-9-BBN, trivinylborane and dichlorovinylborane also demonstrated that the electronic effects caused by the boron atom are overridden by steric factors and the corresponding TSs adopt classical [4 + 2] character.[15]

In a related report, Carreaux, Cossío and co-workers[16] described the experimental and computational study of the mechanism of the thermal dimerization of 2-boryl-1,3-butadienes. To explain the evolution of the [4 + 3] TSs toward the [4 + 2] cycloadducts, the frontier molecular orbital (FMO) approach in conjunction with the second-order perturbation

[a]*Instituto de Química Rosario (CONICET), Facultad de Ciencias Bioquímicas y Farmacéuticas, Universidad Nacional de Rosario, Suipacha 531, Rosario (2000), Argentina. E-mail: vallejos@iquir-conicet.gov.ar, pellegrinet@iquir-conicet.gov.ar*
[b]*Laboratorio de Estructura Molecular y Propiedades, Área de Química Física, Departamento de Química, Facultad de Ciencias Exactas y Naturales y Agrimensura, Universidad Nacional del Nordeste, Avda. Libertad 5460, (3400) Corrientes, Argentina*

†Electronic supplementary information (ESI) available: Distances, topological properties and electron population along the IRC coordinates. See DOI: 10.1039/c3ob41571f

theory were used. In the early stage of the reaction the σ-overlap between the 2p atomic orbitals was more stabilizing for the C–B interaction than for the C–C counterpart, favoring the [4 + 3] pathway. However, beyond the TS the C–C orbital interaction became more favorable and the [4 + 3] zwitterionic species easily fell to the [4 + 2] cycloadduct.

Apart from the classical approach, the quantum theory of atoms in molecules (QTAIM)[17,18] based on the topological analysis of the electron charge density allows one to predict the structure and the stability of a molecular system. The properties of the charge density at a bond critical point (bcp) are useful to characterize the static and dynamic properties and the nature of a bonding interaction. Moreover, the electronic effects predicted by this theory can be assessed by the observable electron density. In addition, the QTAIM topological analysis of the electron density along the reaction pathway has been demonstrated to be a powerful tool for characterizing reactions and understanding the nature of key interactions. For example, this approach has been used to study the dimerization of cyclopentadiene,[19] the Cope rearrangement of 1,5-hexadiene[20] and other pericyclic and pseudopericyclic reactions.[21–27] Furthermore, this analysis has been used to understand the changes in the breaking and forming bonds in other types of reactions such as bimolecular nucleophilic substitutions,[28] cycloadditions catalyzed by Lewis acids,[29] alkene protonations catalyzed by zeolite,[30] *etc*. Although the QTAIM topological analysis along the course of the reaction has been applied to study a wide variety of chemical transformations, to our knowledge it has not yet been used to investigate the DA reactions of unsaturated organoboron dienophiles. In the present work we report the results of such an analysis for the DA reactions of vinylboranes in order to gain a better understanding about the mechanism, particularly about the electron reorganization in the evolution of the [4 + 3] TSs toward the [4 + 2] products.

Methodology

The geometries of the reactants, the TSs and the products were optimized without any constraints. Hybrid density functional theory (DFT) calculations at the Becke3 Lee–Yang–Parr (B3LYP) level[31,32] with the 6-311++G(d,p) basis set were carried out using the Gaussian 03 suite of programs.[33] Frequency calculations were performed to verify the nature of the stationary points: TSs had one imaginary frequency and the reactants and the cycloadducts had no imaginary frequencies. Zero-point vibrational energies (ZPVEs) were computed with the B3LYP/6-311++G(d,p) method and were not scaled. Starting from the TSs obtained for each process, intrinsic reaction coordinate (IRC) calculations were computed to verify the connectivity with reactants and products using a step size of 0.10 Bohr. For the QTAIM topological analysis total electron densities were calculated at the B3LYP/6-311++G(d,p) level of theory. The bond and atomic properties were calculated using the AIMALL program.[34]

Results and discussion

The DA reactions of isoprene with vinylborane (**1**), dimethylvinylborane (**2**) and dichlorovinylborane (**3**) were chosen to analyze the effect of the substituent on boron on the reaction mechanism (Scheme 1). Such reactions may lead to two regioisomeric products (*meta* **P-M** and *para* **P-P**) through four different TSs: *meta endo* (**TS-MN**), *meta exo* (**TS-MX**), *para endo* (**TS-PN**) and *para exo* (**TS-PX**). The structures involved in the DA reactions of isoprene with vinylboranes **1–3** were previously optimized using the HF/6-31G* and the B3LYP/6-31G* levels of theory.[14,15] We have re-examined the geometries and the energetics using B3LYP/6-311++G(d,p). Overall, our results agreed with those reported before. Consequently, in this work we focused on the theoretical discussion of the change in the distributions of the charge density.

Selected geometric and energetic parameters (activation energies ($\Delta E^{\#}$), Gibbs activation energies ($\Delta G^{\#}$), and reaction energies (ΔG)) for the DA reactions under study are collected in Table 1.

Regarding the nature of the substituent attached to boron, the calculated activation energy increased in the order **1** < **3** < **2**. As has been found before, *endo* pathways were favored for all reactions. For the reaction of vinylborane (**1**), an unusual predominance of the *meta* product was predicted, whereas for the reactions with the other dienophiles the formation of the *para* cycloadducts was more favorable in agreement with experimental results.[12,35] The calculated *para* regioselectivity was higher for the reaction of dichlorovinylborane (**3**) than for the reaction of dimethylvinylborane (**2**).

All the TSs were asynchronous with the C_2–C_3 distances being shorter than the C_1–C_6 distances. In addition, the TSs with chloro substituents on the boron atom showed higher asynchronicities than their methyl analogues. In the *endo* TSs of the reaction with vinylborane (**1**) (**TS-1MN** and **TS-1PN**) the C_6–B distances were much shorter than the C_1–C_6 distances, denoting a strong [4 + 3] character, while for *exo* TSs and the *endo* TSs of dimethylvinylborane (**2**) C_1–C_6 and C_6–B distances were similar. The *exo* TSs of dimethylvinylborane (**2**) and all the TSs of dichlorovinylborane (**3**) had [4 + 2] character, the

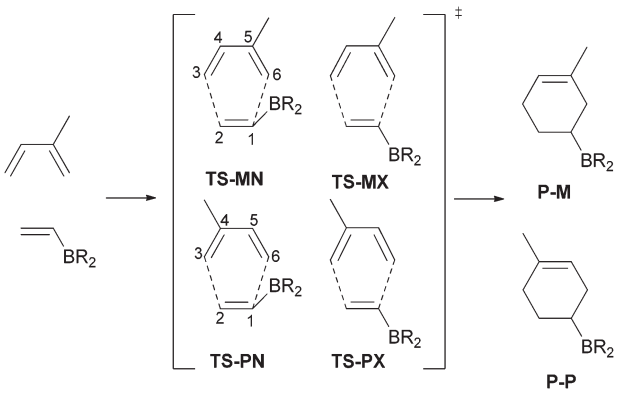

Scheme 1

Table 1 B3LYP/6-311++G(d,p) geometric and energetic parameters

	R (Å)								
TS	C_1–C_6	C_2–C_3	C_6–B	$\Delta E^{\#}$ (kcal mol^{-1})	$\Delta G^{\#}$ (kcal mol^{-1})	*meta*/*para* ratio[a]	Products	ΔE (kcal mol^{-1})	ΔG (kcal mol^{-1})
1M	2.608	2.156	1.972	12.24	25.18	Calcd 75 : 25	**1P-M**	−25.48	−12.67
1MX	2.616	2.059	2.536	18.09	30.35	Exp. —			
1PN	2.614	2.126	2.195	13.17	25.85		**1P-P**	−25.48	−12.67
1PX	2.653	2.059	2.648	17.43	29.67				
2MN	2.566	2.062	2.598	19.71	33.53	Calcd 29 : 71	**2P-M**	−26.33	−12.91
2MX	2.520	2.067	2.788	21.44	34.29	Exp. 39 : 61[35]			
2PN	2.592	2.084	2.653	19.28	32.98		**2P-P**	−26.32	−12.51
2PX	2.561	2.069	2.842	20.87	33.95				
3MN	2.647	2.020	2.765	17.05	30.21	Calcd 14 : 86	**3P-M**	−32.71	−14.34
3MX	2.628	2.018	2.920	18.54	31.20	Exp. 40 : 60[12]			
3PN	2.691	2.033	2.820	16.20	29.16		**3P-P**	−32.65	−14.33
3PX	2.682	2.016	2.983	17.46	29.86				

[a] Ratios were computed using Boltzmann factors based on $\Delta G^{\#}$ and considering both *endo* and *exo* TSs for each regiochemistry.

C_1–C_6 distances being shorter than the C_6–B distances. In addition, IRC calculations confirmed that all reactions under study were concerted.

Analysis of the electron charge density of the TSs

Several topological parameters evaluated at the bcp can be used to obtain information about the nature and features of the chemical bonds between the interacting species. The electron density (ρ_b) at the bcp reflects the strength of a bond and its Laplacian ($\nabla^2\rho_b$) measures the local charge concentration ($\nabla^2\rho_b < 0$) or local charge depletion ($\nabla^2\rho_b > 0$).[17,18] These two properties along with the relationship $|V_b|/G_b$ (wherein V_b and G_b are the potential and the kinetic energy densities at the bcp, respectively) and the total energy density (H_b) are used to analyze the covalent character of an interaction.[36] In addition, the ellipticity, defined as $\varepsilon = \lambda_1/\lambda_2 - 1$ (where λ_1 and λ_2 are the negative eigenvalues of the Hessian of the electron density with respect to the position, that is, the curvatures of the density at the bcp perpendicular to the bond path), evaluated at bcp gives information about the charge distribution around the bond path, and it can be employed to determine the π character of a bond and also its stability.[24]

Another parameter often used in the study of a bonding interaction is the delocalization index (DI). This parameter indicates the extent of exchange of electrons between two atomic basins and it can be calculated between two atoms bonded by a bond path or without having a bond path to analyze the different interactions present in TSs.[37] Fig. 1 shows the molecular graphs of the TSs for the four different modes of addition between the diene and the dienophiles. The topological properties evaluated at the selected bcps are listed in Table 2, where DIs are also included.

The TSs corresponding to the reactions of isoprene with **2** and **3** and the *exo* TSs of the reaction with **1** exhibited two new bcps associated with forming C_1–C_6 and C_2–C_3 σ-bonds and a ring critical point (rcp) related to the six-membered cyclic structure of these TSs (Fig. 1). The topological pattern is in line with that reported by Rode and Dobrowolski for the TSs of pericyclic reactions.[21–23] Interestingly, the *endo* TSs of the reaction with **1** (**TS-1MN** and **TS-1PN**) showed a particular topological pattern, since the C_2–C_3 and C_6–B bcps are involved in a seven-membered cyclic structure with the corresponding rcp. However, contrary to the reported results for other cycloaddition reactions, the C_6–B bond path and the associated bcp do not lead to the formation of a σ-bond. The expected bcp associated with the formation of the C_1–C_6 σ-bond and the resulting six-membered ring was not found though. This surprising topological pattern supports the non-classical [4 + 3] character attributed to these TSs.

It is important to remark that these results demonstrate that TSs with C_6–B distances shorter than C_1–C_6 distances, such as **TS-1MX** and **TS-1PX**, do not necessarily exhibit C_6–B bcps and, therefore, should not be directly associated with the [4 + 3] mechanism. The analysis of the electron charge distribution of the TSs such as the one performed herein appears to give a more accurate description of the nature of TSs.

For all the TSs under study, the values of the ρ_b at C_2–C_3 bcp lie in the range of 0.059–0.080 au, $\nabla^2\rho_b > 0$ (0.019–0.041 au); $|V_b|/G_b > 1$ (1.554–1.831) and $H_b < 0$ (Table 2). These properties indicate that the nature of the C_2–C_3 interaction is partially covalent.[36,38] In addition, ellipticity values at the C_2–C_3 bcp are close to zero, which indicates that the distribution of the electron density around the interaction line connecting both atoms is almost symmetrical. The ρ_b values at the C_2–C_3 bcp are a little higher in the TSs corresponding to the reaction with dichlorovinylborane (**3**) relative to those for the reaction with dimethylvinylborane (**2**), resulting in a slight strengthening of the C_2–C_3 interaction in the first case.

For the TSs of the reactions with **2** and **3** and for the *exo* TSs of the reaction with **1** ρ_b at C_1–C_6 bcp lie in the range of 0.023–0.032 au and $\nabla^2\rho_b > 0$ (0.043–0.050 au). The values of ρ_b at the C_1–C_6 bcp are smaller than those at the C_2–C_3 bcp and DI C_1–C_6 are approximately half of DI C_2–C_3 which is in accordance with the calculated interatomic distances,

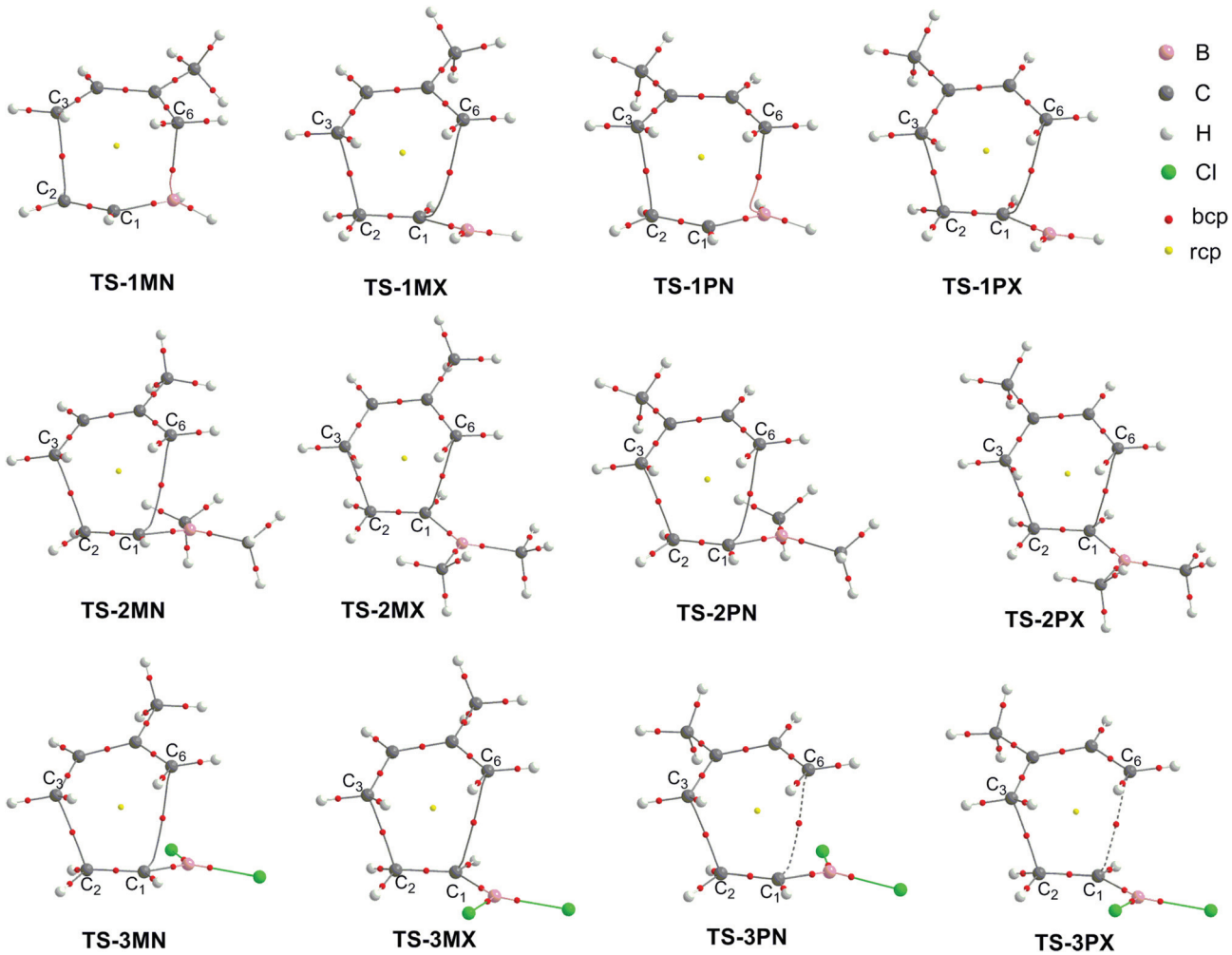

Fig. 1 Molecular graphs of the TSs corresponding to the four modes of addition between isoprene and vinylborane (**1**), dimethylvinylborane (**2**) and dichlorovinylborane (**3**).

Table 2 Local topological properties for the selected bond critical point and delocalization indexes (DI)[a]

	ρ_b (au)		$\nabla^2\rho_b$ (au)		ε		$\lvert V_b\rvert/G_b$		H_b (au)		DI		
TS	C_6–X	C_2–C_3	C_6–X	C_2–C_3	C_6–X	C_2–C_3	C_6–X	C_2–C_3	C_6–X	C_2–C_3	C_1–C_6	C_2–C_3	C_6–B
1MN	0.0709	0.0586	−0.0381	0.0406	0.2763	0.0636	2.3551	1.5543	−0.0363	−0.0126	0.23	0.41	0.28
1MX	0.0306	0.072	0.0475	0.0265	0.9467	0.0701	1.0643	1.7483	−0.0008	−0.0197	0.28	0.47	0.07
1PN	0.0466	0.0629	0.0233	0.0369	0.5461	0.0418	1.6538	1.6147	−0.0110	−0.0147	0.24	0.43	0.17
1PX	0.0270	0.0725	0.0464	0.0270	0.8790	0.0689	0.9941	1.7451	0.0001	−0.0197	0.26	0.47	0.06
2MN	0.0314	0.0720	0.0503	0.0281	1.0271	0.0479	1.0696	1.7349	−0.0009	−0.0195	0.28	0.47	0.06
2MX	0.0317	0.0716	0.0481	0.0281	0.4104	0.0830	1.1100	1.7322	−0.0015	−0.3021	0.30	0.46	0.03
2PN	0.0293	0.0691	0.0493	0.0317	0.9036	0.0553	1.0377	1.6930	−0.0005	−0.0179	0.26	0.45	0.06
2PX	0.0291	0.0714	0.0471	0.0288	0.4433	0.0800	1.0642	1.7257	−0.0008	−0.0191	0.28	0.46	0.03
3MN	0.0264	0.0781	0.0470	0.0199	1.1066	0.0529	0.9863	1.8228	0.0002	−0.0231	0.24	0.49	0.06
3MX	0.0259	0.0785	0.0448	0.0196	0.5209	0.0762	1.0115	1.8264	−0.0001	−0.0233	0.25	0.49	0.03
3PN	0.0241	0.0764	0.0453	0.0228	0.9974	0.0572	0.9494	1.7942	0.0005	−0.0220	0.22	0.48	0.05
3PX	0.0232	0.0791	0.0433	0.0192	0.6053	0.0732	0.9583	1.8312	0.0004	−0.0236	0.23	0.49	0.03

[a] For **TS-1MN** and **TS-1MX**, X = B and for the remaining TSs, X = C_1. See Fig. 1 for atom numbering.

consequently these properties also reflect the asynchronicity of the TSs. Interestingly, for the reaction with **2** and **3** the ellipticity at the C_1–C_6 bcp takes relatively high values (ε = ~1) in *endo* TSs while in *exo* TSs ε < 0.6. The latter are similar to those found for the DA reaction of ethene with 1,3-butadiene.[26] These results suggest that the presence of the boron atom affects the electron distribution of its surrounding environment, particularly in the *endo* modes of addition.

Furthermore, from the molecular graphs it can be noted that the C_2–C_3 bond paths are rather linear whereas the C_1–C_6 bond paths present a considerable bend. Hence, the topological parameters show that formation of the C_2–C_3 bonds is more advanced than the bonding between C_1 and C_6. In the TSs of the reaction with dimethylvinylborane (**2**) the values of ρ_b at the C_1–C_6 bcp are higher than those in the TSs for dichlorovinylborane (**3**). In addition, at this bcp $|V_b|/G_b > 1$ and $H_b < 0$ for the former, whereas $|V_b|/G_b < 1$ and $H_b > 0$ for the TSs corresponding to **3** (except **TS-3MN**). In contrast to the observation for the C_2–C_3 bcp, these data indicate that the C_1–C_6 interaction is slightly stronger in the TSs of the reaction with dimethylvinylborane (**2**) than those for dichlorovinylborane (**3**). It is also important to note that in all the TSs with [4 + 2] character, the DI C_6–B values are negligible (0.01–0.07) indicating that the C_6–B interaction is very weak.

For the particular case of **TS-1MN**, at the C_6–B bcp ρ_b (0.071 au) has a value higher than that at the C_2–C_3 bcp (0.059 au), $\nabla^2\rho_b < 0$ (−0.0381 au), the potential energy is dominant ($|V_b|/G_b$ = 2.355 au) and $H_b < 0$. These topological properties indicate that the C_6–B interaction in **TS-1MN** is stronger than all the interactions corresponding to the forming bonds in the studied TSs. More importantly, the C_6–B bcp is the only one that displays the hallmarks of "shared-shell" or covalent interaction.

Fig. 2 shows the contour lines of the $-\nabla^2\rho_{(r)}$ superimposed on the molecular graphs for **TS-1MN** and **TS-2PN** as representative models of [4 + 3] and [4 + 2] TSs in which it can be clearly visualized that the charge distribution has different patterns in the plane containing the C_1, C_6 and B atoms. These peculiarities in the topology of the electron density can be useful to distinguish between [4 + 3] and [4 + 2] TSs. In **TS-1MN** (Fig. 2a) there is a region of high concentration of charge density between the C_6 and the B atom, including the C_6–B bcp and a charge depletion zone is observed on the C_1 atom. In **TS-2PN** (Fig. 2b) a depletion of charge density between the C_1 and the C_6 atoms is detected and the outermost shell of charge concentration of C_6 exhibits an incipient deformation oriented toward C_1, suggesting, as expected, that during the course of the reaction, electron density will concentrate in the region between C_1 and C_6 to form a covalent interaction.

It is worth nothing that, although there is no C_1–C_6 bond path and its corresponding bcp in **TS-1MN**, the value of DI C_1–C_6 (0.23) is noticeable and similar to DI C_6–B (0.28). This important finding provides evidence that the C_1 and B atoms share electron density with C_6, which confirms the [4 + 3] character of this TS. The highest sharing of charge density between the diene and the dienophile in **TS-1MN** could be considered a key stabilizing factor. **TS-1PN** shows a similar topological pattern of the charge distribution but the C_6–B interaction is weaker and has "closed-shell" features, as shown in Fig. 3. This supports the higher energy of **TS-1PN** relative to **TS-1MN**, but the lower energy relative to the *exo* [4 + 2] TSs (**TS-1MX** and **TS-1PX**).

According to QTAIM, an atom is defined by the nucleus and its atomic basin, which is the volume enclosed by a zero-flux surface filled by the gradient lines of $\rho_{(r)}$ ending up at the nucleus.[17,18] In a molecule, each atomic basin is separated from their neighboring basins by a zero-flux surface in the gradient vector field of the charge density. The atomic electron population $N(\Omega)$ can be obtained by integrating the electron density over the atomic basin, which can be used to calculate the corresponding atomic net charge as $q(\Omega) = N(\Omega) - Z_\Omega$, with Z_Ω being the atomic number.[18,20,39–43] Fig. 4 displays the change in atomic population $\Delta N(\Omega)$ from the isolated reactants to the TSs. The net charges calculated for selected atoms and the charge transfer from the diene to the dienophiles in the TSs are included in Table 3. The accuracy of the integrated properties was tested taking into account that the summation of

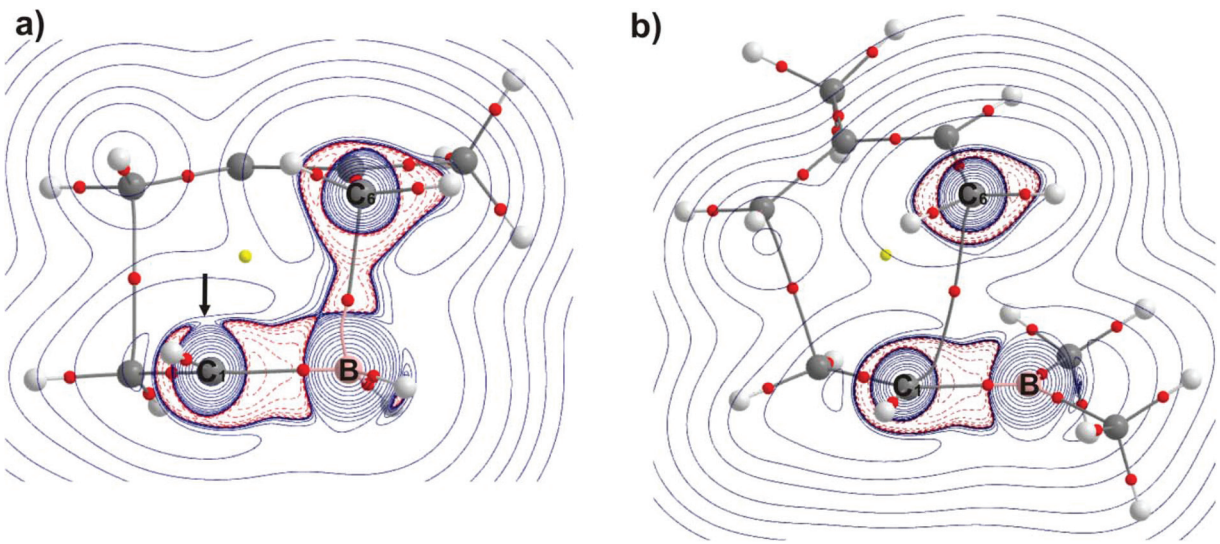

Fig. 2 Contour plots of $-\nabla^2\rho_{(r)}$ in the plane containing C_1, C_6 and the B atom superimposed on the molecular graph of (a) **TS-1MN** and (b) **TS-2PN**. Continuous blue lines and dashed red lines depict regions of local charge density depletion and concentration, respectively. The arrow in Fig. 2a denotes the position of charge depletion at C_1.

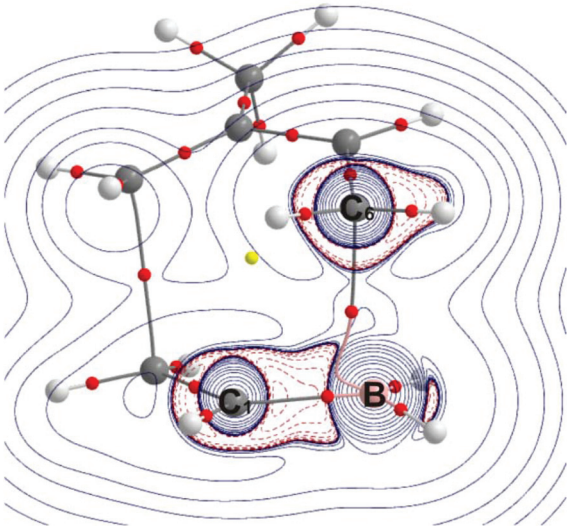

Fig. 3 Contour plot of $-\nabla^2\rho_{(r)}$ in the plane containing C_1, C_6 and the B atom superimposed on the molecular graph of **TS-1PN**. See Fig. 2 for key.

the atomic electron population values for each molecule reproduces the total electron population within 0.001 au. In addition, all the integrated atomic properties were obtained with the values of $|N(\Omega)|$ less than 4×10^{-4} for the non-hydrogen atoms and less than 10^{-5} for the hydrogen atom as specified in the literature.[44]

From a simple visual analysis of the changes in the $N(\Omega)$ (Fig. 4), it is observed that the population of the atoms were more significantly affected when passing from the isolated reactants to the TSs in **TS-1MN** and **TS-1PN**, in particular for C_1, C_6 and B. This reflects the striking electron redistribution that occurs in the TSs with [4 + 3] character. In these TSs, C_1 loses electron population and hence its negative net charge decreases (Table 3), whereas the C_6 and the B atom gain electron population causing an increase of the negative net charge in the first and a decrease in the positive net charge in the second. In contrast, in the [4 + 2] TSs C_1 gains electron population and its net charge becomes more negative. As in [4 + 3] TSs, the electron population of the B atom also becomes higher particularly in *endo* TSs, but to a lesser extent. The C_6

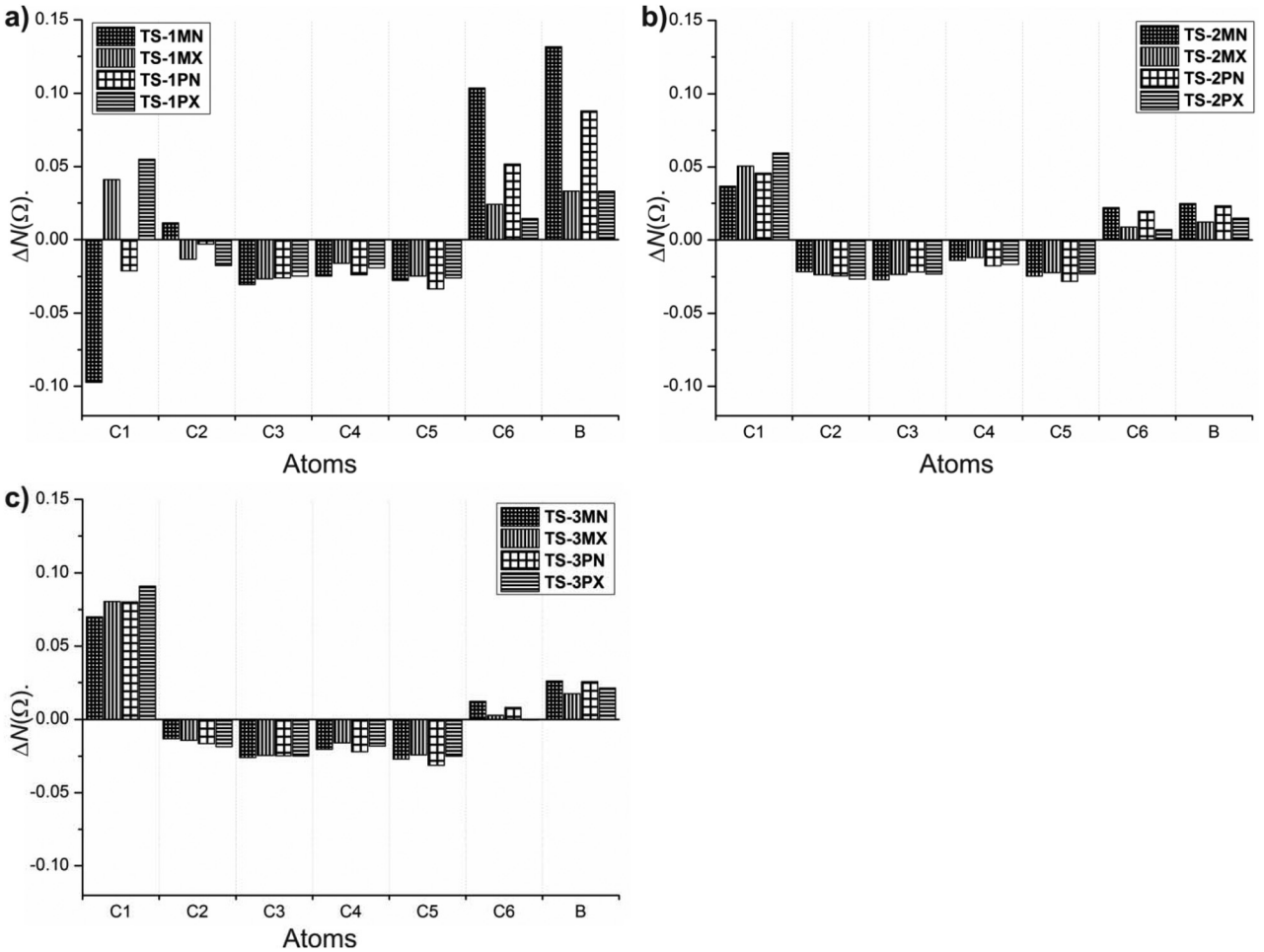

Fig. 4 Variation of atomic populations ($\Delta N(\Omega)$, in au) for selected atoms in the TSs with respect to reactants for the reactions of isoprene with (a) vinylborane (**1**), (b) dimethylvinylborane (**2**) and (c) dichlorovinylborane (**3**).

Table 3 Net charges for selected atoms and charge transfer from the diene to the dienophiles for the TSs under study (in *e*)

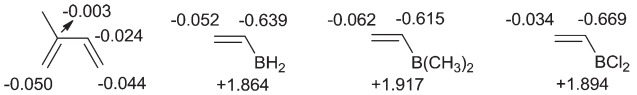

TS	Q(B)	q(C_1)	q(C_2)	q(C_3)	q(C_4)	q(C_5)	q(C_6)	CT[a]
1MN	+1.732	−0.542	−0.063	−0.013	+0.001	+0.025	−0.153	0.072
1MX	+1.831	−0.680	−0.039	−0.017	−0.008	+0.022	−0.074	0.116
1PN	+1.776	−0.618	−0.049	−0.024	+0.021	+0.010	−0.095	0.118
1PX	+1.831	−0.694	−0.034	−0.025	+0.016	+0.002	−0.058	0.130
2MN	+1.892	−0.652	−0.041	−0.017	−0.010	+0.022	−0.072	0.082
2MX	+1.905	−0.666	−0.039	−0.020	−0.012	+0.019	−0.058	0.074
2PN	+1.894	−0.661	−0.038	−0.028	+0.015	+0.004	−0.063	0.091
2PX	+1.902	−0.675	−0.036	−0.027	+0.014	−0.001	−0.051	0.089
3MN	+1.868	−0.739	−0.021	−0.018	−0.004	+0.024	−0.062	0.154
3MX	+1.876	−0.749	−0.020	−0.019	−0.008	+0.021	−0.052	0.149
3PN	+1.868	−0.749	−0.017	−0.025	+0.019	+0.007	−0.052	0.174
3PX	+1.873	−0.760	−0.015	−0.025	+0.015	+0.001	−0.044	0.168

[a] Charge transfer values were computed as the addition of the individual charges of all the atoms in the isoprene moiety.

atom experiences a slight increase in the population, which is more evident in *endo* TSs. The change in N(C_6) from reactants to TSs decreases in the order vinylborane (**1**) > dimethylvinylborane (**2**) > dichlorovinylborane (**3**). The negligible increase in the electron population on C_6 for **3** is a consequence of the weak interaction with C_1.

In general, the electron populations on C_2, C_3, C_4 and C_5 decrease due to the delocalization of "π" electron charge density on the other atoms. Therefore, the charge redistribution in the TSs involves a charge density displacement toward the region of the C_1, C_6 and B atoms, *i.e.* toward the site where the C_1–C_6 bond is being formed.

The charge transfer (CT) between the fragments corresponding to the reactants in the TSs was computed considering the addition of the individual charges of the atoms in the isoprene moiety. As expected, for all the TSs the positive sign of the CTs indicate that an electronic flow from the diene toward the dienophile occurs. Surprisingly, the CT in the TS with the lowest energy barrier (**TS-1MN**) is the smallest (0.072 *e*). This result is in contrast to the proposal that an increase in the calculated CT is associated with a decrease in the energetic barrier for DA reactions.[45,46] However, for the reactions of isoprene with dienophiles **2** and **3** a linear correlation between the activation energy and the CT with R^2 = 0.96 is obtained (Fig. 5). The lack of correlation for the DA reaction of vinylborane (**1**) might be related to the peculiar electron distribution of the TSs, particularly for those with [4 + 3] character. This supports previous results from our group which indicated that for some DA reactions of unsaturated boranes CT values did not correlate well with activation energies. Therefore, care should be exercised when estimating reactivity trends from CT.[47]

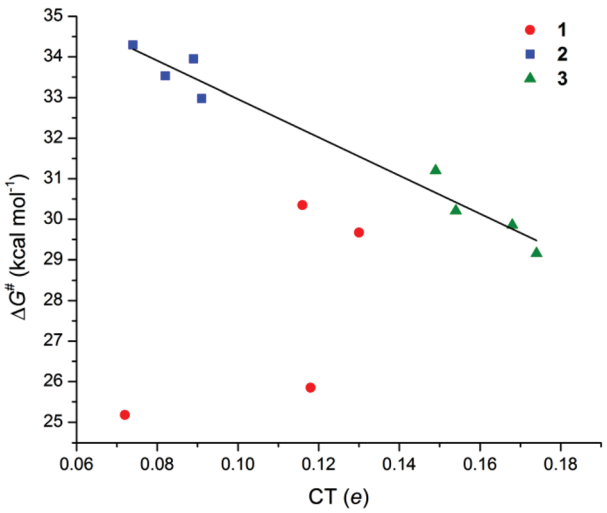

Fig. 5 Activation free energy ($\Delta G^{\#}$) *vs.* charge transfer (CT) for the TSs of the DA reactions of isoprene with vinylborane (**1**), dimethylvinylborane (**2**) and dichlorovinylborane (**3**). For **2** and **3**, R^2 = 0.96.

Evolution of the local properties of $\rho_{(r)}$ and the atomic population along the reaction path

The analysis of the variation of the topological properties and the atomic populations along the reaction coordinate provides interesting information about bond formation in the DA reactions. Therefore, a better understanding about the key changes in the electron density in the evolution of the [4 + 3] TSs towards the [4 + 2] products associated with the reaction of isoprene with vinylborane (**1**) can be obtained. For the remaining reactions under study, this approach was carried out to assess the effect of the substituent and the mode of addition on the distribution of the electron density in the course of the reaction.

The variation of the several topological properties at the C_1–C_6, C_2–C_3 and C_6–B bcps along the reaction coordinate associated with **TS-1MN** and **TS-2PN** TSs as models of [4 + 3] and [4 + 2] TSs, respectively, are displayed in Fig. 6. The results for the remaining TSs are reported in the ESI.† Fig. 6a shows that the C_6–B bcp is present from the early stages of

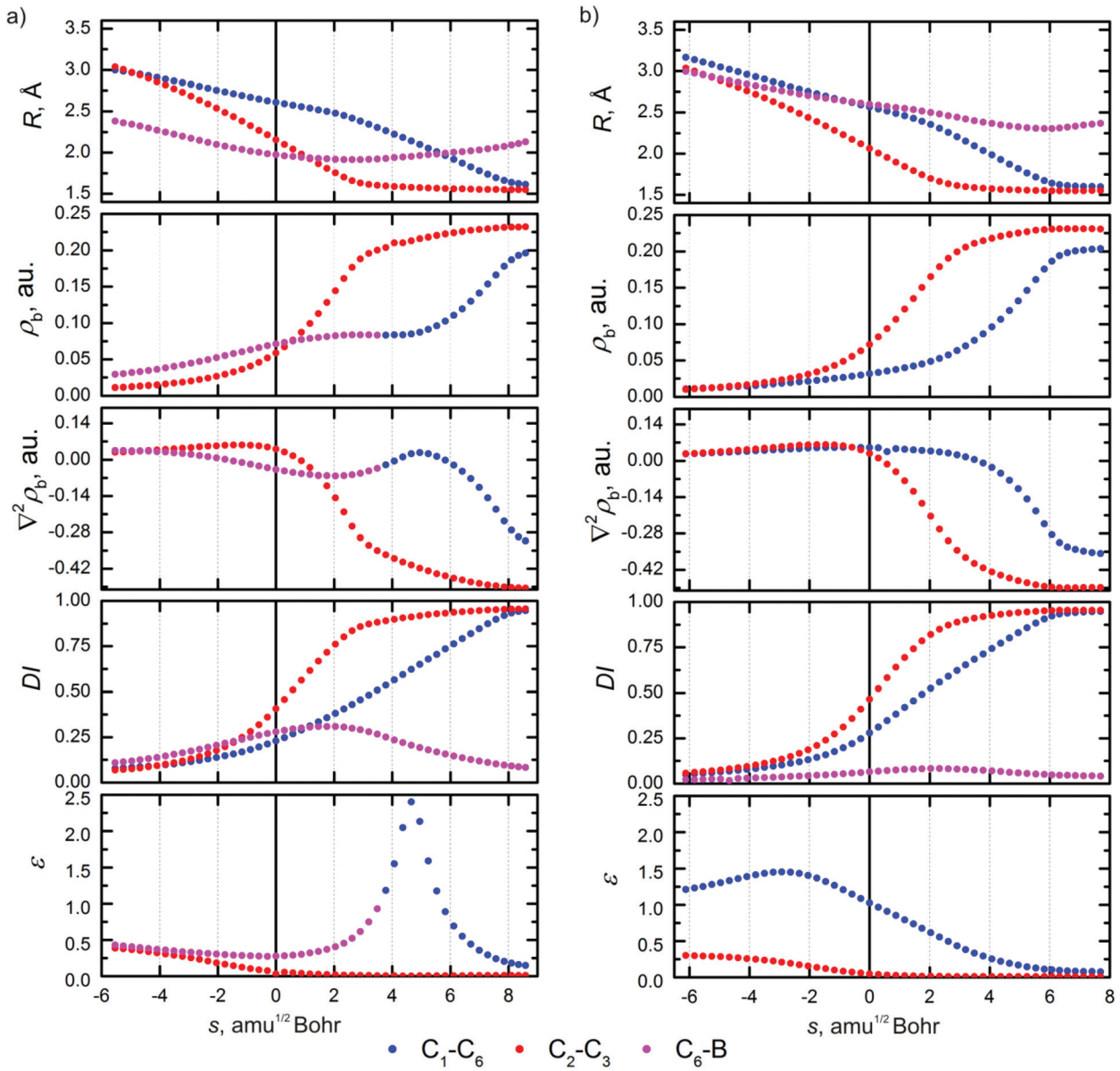

Fig. 6 Distances, topological properties and delocalization indexes along the IRC path corresponding to (a) **TS-1MN** and (b) **TS-2PN**. TSs are located at s = 0.0 amu$^{1/2}$ Bohr.

the reaction coordinate associated with **TS-1MN**. At this bcp ρ_b increases until steps after the TS, $\nabla^2\rho_b$ takes small positive values and decreases very slowly, changing its sign near the point at −1.5 amu$^{1/2}$ Bohr of the reaction coordinate corresponding to a C_6–B distance of 2.06 Å. This indicates that at this point, the C_6–B interaction changes from a closed-shell interaction ($\nabla^2\rho_b > 0$) to a shared-shell interaction ($\nabla^2\rho_b < 0$). The DI C_6–B shows a bell-shaped profile, with a maximum value of 0.31 that appears after the TS at 1.8 amu$^{1/2}$ Bohr where the C_6–B distance is the shortest (1.91 Å). It is interesting to note that in the early stages of the reaction (from −5.6 to −1.0 amu$^{1/2}$ Bohr) the DI C_6–B is relatively low (0.1–0.2), but is greater than DI C_1–C_6 and DI C_2–C_3. In addition, the C_6–B distance (2.40–2.04 Å) is shorter than C_1–C_6 (3.00–2.69 Å) and C_2–C_3 (3.03–2.38 Å) distances. These results indicate that at initial stages of the reaction the C_6 and B atomic basins are in a preferential position for sharing their electrons. Hence, the C_6–B interaction seems to play a crucial role, facilitating the formation of the new σ-bonds between the diene and the dienophile. Furthermore, in the early steps of the reaction coordinate the DI C_1–C_6 increases slowly and from 1.5 amu$^{1/2}$ Bohr (coincident with the maximum value of DI C_6–B) the change is more pronounced. From that point, and DI C_1–C_6 becomes greater than DI C_6–B, which begins to fall gradually towards the formation of the cycloadduct. Although the sharing of electrons between C_1 and C_6 becomes more favorable, the corresponding bcp has not appeared yet.

At 3.48 amu$^{1/2}$ Bohr, the ρ_b at C_6–B bcp is relatively low, $\nabla^2\rho_b$ has a small negative value, the DI C_6–B is decreasing and the ε begins to increase, which denotes an instability of the C_6–B bonding interaction. At this stage, a change of the topological pattern occurs since the C_6–B bcp disappears and the C_1–C_6 bcp appears. However, the C_6–B distance (1.92 Å) is still shorter than the C_1–C_6 distance (2.30 Å). To achieve a more complete understanding about the mechanism of the sudden change in the topological pattern between the last structure with the C_6–B bcp (**1MN-p14**) and the first structure with the C_1–C_6 bcp (**1MN-p15**), we calculated intermediate structures by reducing the step size of the IRC to 0.01 Bohr between 3.48 and 3.78 amu$^{1/2}$ Bohr. The contour plots of the $-\nabla^2\rho_{(r)}$ for these structures plus two additional borderline structures next to the conflict structure (denoted as **1MN-p-14i** and **1MN-p-15i**) are displayed in Fig. 7.

At **1MN-p-14i** the trajectory of the bond path linking C_6 and B is almost coincident with the C_1–B bond path from the B atom to the C_1–B bcp, and then at this point it bends abruptly towards C_6. In the following structure, **1MN-p-15i** the C_6–B bcp disappears and the C_1–C_6 bcp appears, leading to a six-member ring structure. At this point, the C_1–C_6 bond path has the same trajectory as the C_1–B bond path from C_1 to the C_1–B bcp, and then it turns in the direction leading to the C_6 atom. These results suggest that at some point along the reaction coordinate C_6 and the C_1–B bcp should be connected through a bond path. Based on the QTAIM approach, these interesting findings can be interpreted as the system passing through an energetically and topologically unstable conflict structure, where the B and C_1 atoms are competing to be the attractor of the charge density localized on the bond path that connects with C_6.[48] The conflict structure constitutes a key point in the evolution of the [4 + 3] structure toward the [4 + 2] structure where the C_1–C_6 bcp, associated with the C_1–C_6 σ-bond in the cycloadduct appears. Unfortunately, we have not been able to locate such a conflict structure.

After the conflict point and until 4.7 amu$^{1/2}$ Bohr ρ_b at the C_1–C_6 bcp remains almost constant and has a value of less than 0.10 au, but the $\nabla^2\rho_b$ increases slightly, becoming positive and the ellipticity sharply increases reaching a maximum

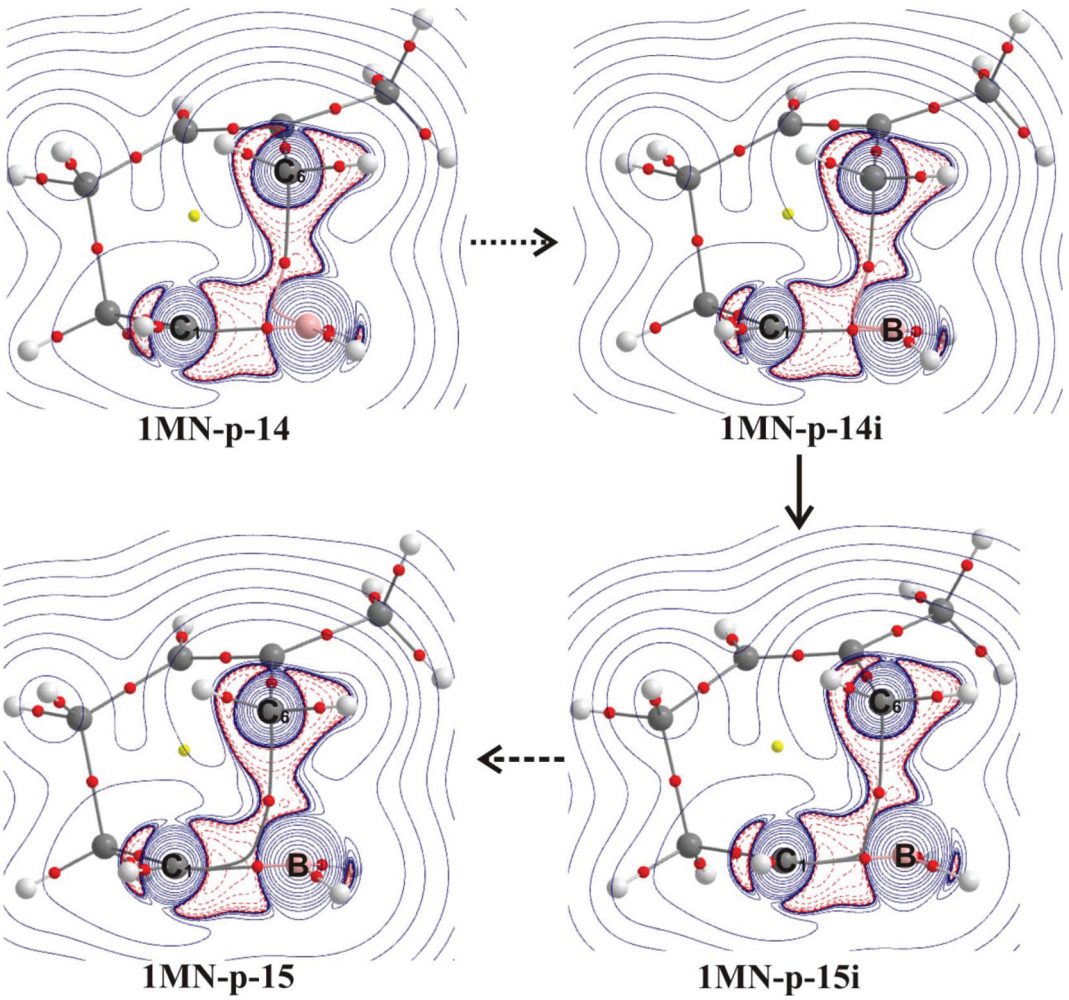

Fig. 7 Contour plots of $-\nabla^2\rho_{(r)}$ in the plane containing the C_1, C_6 and B atoms superimposed on the molecular graphs of selected structures along the reaction coordinate corresponding to **TS-1MN**.

of 2.40. These results denote that in the internuclear region between C_1 and C_6, a striking electron redistribution occurs, which facilitates the nuclear displacement necessary for the C_1–C_6 σ bond formation.

After 4.7 amu$^{1/2}$ Bohr the C_1–C_6 distance becomes shorter than the C_1–B distance and at the C_1–C_6 bcp ρ_b increases gradually up to *ca.* 0.20 au, $\nabla^2\rho_b$ becomes more negative and the ellipticity decreases abruptly to nearly zero. Hence, in this part of the reaction coordinate the accumulation of charge density in the internuclear region C_1–C_6 increases progressively in order to reinforce the C_1–C_6 interaction to form the covalent bond present in the cycloadduct.

In general, the trends of the topological properties along the IRC for **TS-1PN** were similar to those for **TS-1MN**, but the changes were less pronounced (see the ESI†). Accordingly, $\nabla^2\rho_b$ at the C_6–B bcp has positive values along the course of the reaction, indicating a depletion of charge density at the bcp, and in the early stage of the reaction DI C_6–B is as low as DI C_6–C_1 and DI C_2–C_3, and then at −1.7 amu$^{1/2}$ Bohr (before the TS) DI C_6–B < DI C_1–C_6. In addition, the conflict structure appears closer to the TS (at 1.5 amu$^{1/2}$ Bohr). It is important to note that the ellipticity at the C_1–C_6 bcp shows a similar profile, reaching a maximum value of 2.0 after the TS. This can be considered a distinctive feature of the reaction pathways associated with a [4 + 3] structure, which is different from the profiles of the ellipticity in the course of the remaining channels under study associated with [4 + 2] structures and other DA reactions reported in the literature. This issue is discussed in further detail below.

For the *exo* TSs of the reaction of **1** and all the TSs for **2** and **3**, ρ_b at the C_1–C_6 bcp and DI C_1–C_6 are low in the early stages of the reaction coordinate and increase gradually with the strengthening of the interaction but later than those for the C_2–C_3 bcp. Also, $\nabla^2\rho_b$ at the C_1–C_6 bcp is positive in the first steps and after ∼4 amu$^{1/2}$ Bohr it decreases and becomes negative, indicating a change in the nature of the C_1–C_6 interaction from closed-shell to shared-shell interaction. Moreover, the DI C_6–B is low throughout the course of the reaction reflecting the weak nature of the secondary orbital interaction between the C_6 and the B atom.

The ellipticity at the C_1–C_6 bcp varies along the reaction coordinate according to the mode of addition (*endo* or *exo*) and the nature of the substituent on the dienophile. For the pathways associated with *endo* TSs, the ellipticity increases in the first stages of the reaction up to a maximum (1.45, 1.20, 1.94 and 1.49 for **TS-2MN**, **TS-2PN**, **TS-3MN** and **TS-3PN**, respectively) before the TS (at ∼−3 amu$^{1/2}$ Bohr) and then it decays smoothly. These maxima show higher values of ε for *meta* TSs and for dichlorovinylborane (**3**). For *exo* TSs, the ellipticity shows relatively high values in the early stages, decreasing progressively towards product formation, with no maximum being observed (see the ESI†).

Several studies have shown that the ellipticity profile evaluated at the bcp corresponding to a forming or breaking bond along the reaction coordinate constitutes a good indicator for distinguishing pseudopericyclic and pericyclic reactions within electrocyclic[24,25] and [2 + 2] cycloaddition reactions.[21–23] In addition, for the [4 + 2] cycloaddition reactions of butadiene and cumulenes with ethylene, formaldehyde and other heteroatomic analogues, it has been found that the values of the ellipticity are below 0.5, and this parameter does not display any maximum during the course of the reaction.[26] Silva and de Lera[25] reported that this pattern in the ellipticity profile indicated that the electron density undergoes only small changes in the course of the DA reaction.

Nevertheless, our results suggest that for the DA reactions of the boron-substituted dienophiles under study, the ellipticity profile could be used as a parameter to differentiate the pathways associated with [4 + 3] or [4 + 2] TSs and within the latter it is possible to distinguish between *endo* and *exo* modes of addition.

In general, for all the reactions under study the profiles of the topological properties at the C_2–C_3 bcp along the course of the reaction show a similar pattern. In the first part of the reaction path, ρ_b at the C_2–C_3 bcp and DI C_2–C_3 increase slightly, and then near the TS the increase becomes more pronounced up to a constant value of ∼0.2 au and 1.0, respectively. $\nabla^2\rho_b$ at the C_2–C_3 bcp varies slightly above zero until immediately after the TS, when it becomes negative and decreases abruptly down to a value of ∼−0.4. The ellipticity at the C_2–C_3 bcp is low (<0.5) before the TS and then decreases to almost zero. These results reinforce the fact that the formation of the C_2–C_3 σ bond occurs earlier than that of the C_1–C_6 σ-bond and furthermore they demonstrate that the charge density in the region of the C_2–C_3 bond is less affected by the substituent. It is important to mention that very little change occurs in the topological properties at the other bcp (C_1–C_2, C_3–C_4, C_4–C_5, C_5–C_6 and C_1–B).

The variations of the electron population of selected atoms along the reaction coordinate for **TS-1MN** and **TS-2PN** are shown in Fig. 8. The results for the remaining TSs under study are displayed in the ESI.†

As noted in the analysis of the TSs, among the analyzed atoms, C_1 has the highest electron population, hence it presents the major negative net charge. Also, C_1 is the atom whose population is more significantly affected along the course of the reaction. For **TS-1MN** and **TS-1PN** the changes in the population of the B atom are almost as important as those for C_1. As expected, the variation of the $N(C_1)$, $N(C_6)$ and N(B) is more significant in the reaction paths for **TS-1MN** and **TS-1PN** than in those for the [4 + 2] TSs.

For **TS-1MN**, initially the atomic populations of C_1 and B respectively decrease and increase and after the TS the first reaches a minimum and the second a maximum simultaneously, concomitant with the largest negative values of $\nabla^2\rho_b$ and with high values of ρ_b at the C_6–B bcp and DI C_6–B. Hence, these results suggest that at this point C_1 transfers charge density to the B atom and consequently the C_6–B interaction becomes stronger.

After this point, the variation of the electronic population of these atoms is reversed. The $N(C_1)$ increases to a maximum and the N(B) decreases to a minimum. As a result, the C_1–C_6

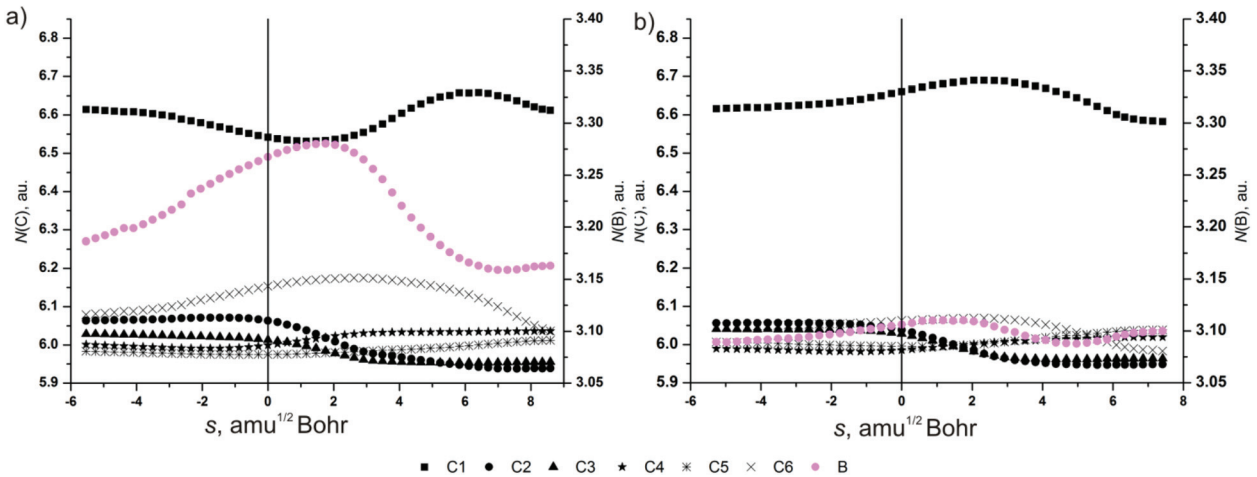

Fig. 8 Electronic population of selected atoms (in *e*) along the IRC path corresponding to (a) **TS-1MN** and (b) **TS-2PN**. The TSs are located at s = 0.0 amu$^{1/2}$ Bohr.

bcp appears. The atomic population of C_6 increases, reaching higher values after the TS and then it decreases abruptly. The change of electron population of C_1 and B are complementary along the reaction coordinate, so a continuous electron transfer between the two atomic basins occur but in two different directions. These results support the assumption that the significant redistribution of the electron density during the course of the reaction is dominated by the electron exchange among C_1, C_6 and B, which is necessary to make the evolution of the [4 + 3] structure to its [4 + 2] counterpart feasible.

In the reaction paths for **TS-1PN** and the [4 + 2] TSs, the changes of the atomic populations are less pronounced. $N(C_1)$, $N(C_6)$ and N(B) remain almost constant and increase slightly beyond the TS (~2 amu$^{1/2}$ Bohr).

It is also interesting to note that $N(C_1)$ and N(B) are higher and vary more along the reaction coordinate for the TSs corresponding to the reaction of dichlorovinylborane (**3**) relative to those for the methyl analogue **2**. Hence, in this case the chlorine atoms seem to have a donating rather than a withdrawing effect towards the more electron-deficient B atom.

Conclusions

The DA reactions of isoprene with vinylborane (**1**), dimethylvinylborane (**2**) and dichlorovinylborane (**3**) have been investigated using density functional theory and the QTAIM approach.

The free energy barriers increased in the order vinylborane (**1**) < dichlorovinylborane (**3**) < dimethylvinylborane (**2**). In addition, for **1** the *meta endo* pathway was favored, while for **2** and **3** the *para endo* mode of addition was preferred. These results are in agreement with the experimental data for the reactions of **2** and **3**. The *endo* TSs of the reaction with vinylborane (**1**) present high [4 + 3] character, while the other TSs under study have [4 + 2] character.

Two topological patterns were found for the different TSs. In the TSs with [4 + 2] character, two bcps appear, corresponding to the C_2–C_3 and C_1–C_6 forming bond and such TSs exhibit a six-membered ring structure. In contrast, in the TSs with [4 + 3] character the C_2–C_3 and C_6–B bcps are found, which are involved in a seven-membered cyclic structure. The C_6–B interaction presents topological features typical of a "shared-shell" interaction whereas the other interactions between the diene and the dienophile show characteristic of "closed-shell" interactions. In addition, the delocalization index values indicated that in **TS-1MN** and **TS-1PN** both C_1 and the B atom share electrons with C_6, demonstrating their [4 + 3] character from the viewpoint of the charge distribution analysis. In addition, in the studied [4 + 2] TSs the C_6–B interaction was weaker. Hence, the higher charge concentration between the diene and the dienophile in the [4 + 3] TSs constitutes a fundamental stabilizing factor.

From the analysis of the variation of the topological properties along the reaction coordinate we found that the *endo* pathways of the DA reaction of isoprene with vinylborane (**1**) display a conflict mechanism. In the evolution of the [4 + 3] structure toward the [4 + 2] structure the system goes through a conflict point, in which the C_1 and B atoms compete to be the attractor of the charge density of the bond path that connects with C_6. The C_6–B interaction, present from the early steps of the DA reaction until beyond the TSs, plays a key role in facilitating the formation of the new σ-bonds.

Along the IRCs of the DA reactions of isoprene with dimethylvinylborane (**2**) and dichlorovinylborane (**3**) and of the *exo* channels for vinylborane (**1**), the topological properties indicated that the C_2–C_3 and C_1–C_6 interactions become stronger during the course of the reaction to form the corresponding σ-bonds, the formation of the former being more advanced than the latter. Throughout the course of all these reactions the C_6–B interaction is weak.

We have found that the profile of the ellipticity at the C_1–C_6 bcp along the IRC may be used as an indicator to differentiate the [4 + 3] and [4 + 2] mechanisms for the DA reactions of boron-substituted dienophiles. Even more, in the latter it is possible to distinguish *endo* and *exo* modes of attack, since a

maximum is found before the TSs for *endo* pathways while no maximum is observed for the *exo* counterparts.

Acknowledgements

We thank CONICET and ANPCyT. M. M. V. and N. M. P. thank UNNE, and SECYT-UNNE. M. M. V. and S. C. P. thank UNR.

Notes and references

1 C. P. Dell, *J. Chem. Soc., Perkin Trans. 1*, 1998, 3873–3905.
2 J. Sauer and R. Sustmann, *Angew. Chem., Int. Ed. Engl.*, 1980, **19**, 779–807.
3 G. Hilt and P. Bolze, *Synthesis*, 2005, 2091–2115.
4 A. M. Sarotti, P. L. Pisano and S. C. Pellegrinet, *Org. Biomol. Chem.*, 2010, **8**, 5069–5073.
5 N. Noiret, A. Youssofi, B. Carboni and M. Vaultier, *J. Chem. Soc., Chem. Commun.*, 1992, 1105–1107.
6 D. A. Evans, W. L. Scott and L. K. Truesdale, *Tetrahedron Lett.*, 1972, **13**, 121–124.
7 D. A. Singleton and J. P. Martinez, *J. Am. Chem. Soc.*, 1990, **112**, 7423–7424.
8 D. A. Singleton and J. P. Martinez, *Tetrahedron Lett.*, 1991, **32**, 7365–7368.
9 D. A. Singleton, J. P. Martinez and G. M. Ndip, *J. Org. Chem.*, 1992, **57**, 5768–5771.
10 D. A. Singleton, J. P. Martinez and J. V. Watson, *Tetrahedron Lett.*, 1992, **33**, 1017–1020.
11 D. A. Singleton, J. P. Martinez, J. V. Watson and G. M. Ndip, *Tetrahedron*, 1992, **48**, 5831–5838.
12 M. Zaidlewicz, J. R. Binkul and W. Sokół, *J. Organomet. Chem.*, 1999, **580**, 354–362.
13 D. A. Singleton, *J. Am. Chem. Soc.*, 1992, **114**, 6563–6564.
14 S. C. Pellegrinet, M. A. Silva and J. M. Goodman, *J. Am. Chem. Soc.*, 2001, **123**, 8832–8837.
15 M. A. Silva, S. C. Pellegrinet and J. M. Goodman, *ARKIVOC*, 2003, 556–565.
16 F. Carreaux, F. Possémé, B. Carboni, A. Arrieta, B. Lecea and F. P. Cossío, *J. Org. Chem.*, 2002, **67**, 9153–9161.
17 R. F. W. Bader, *Atoms in Molecules. A Quantum Theory*, Oxford Science Publications, Clarendon Press, London, 1990.
18 C. F. Matta and R. J. Boyd, *The Quantum Theory of Atoms in Molecules: from solid state to DNA and drug design*, Wiley-VCH, Weinheim, 2007.
19 N. H. Werstiuk and W. Sokol, *Can. J. Chem.*, 2008, **86**, 737–744.
20 E. C. Brown, R. F. W. Bader and N. H. Werstiuk, *J. Phys. Chem. A*, 2009, **113**, 3254–3265.
21 J. E. Rode and J. C. Dobrowolski, *Chem. Phys. Lett.*, 2007, **449**, 240–245.
22 J. E. Rode and J. C. Dobrowolski, *J. Phys. Chem. A*, 2006, **110**, 207–218.
23 J. E. Rode and J. C. Dobrowolski, *J. Phys. Chem. A*, 2006, **110**, 3723–3737.
24 C. S. López, O. N. Faza, F. P. Cossío, D. M. York and A. R. de Lera, *Chem.–Eur. J.*, 2005, **11**, 1734–1738.
25 C. S. López and A. R. de Lera, *Curr. Org. Chem.*, 2011, **15**, 3576–3593.
26 S. Calvo-Losada and J. J. Quirante Sánchez, *J. Phys. Chem. A*, 2008, **112**, 8164–8178.
27 M. Mandado, M. J. González-Moa and R. A. Mosquera, *ChemPhysChem*, 2007, **8**, 696–702.
28 A. Ebrahimi, H. Roohi, M. Habibi, T. Karimian and R. Vaziri, *Chem. Phys. Lett.*, 2006, **419**, 179–183.
29 G. Wagner, T. N. Danks and V. Vullo, *Tetrahedron*, 2007, **63**, 5251–5260.
30 M. Zalazar and N. Peruchena, *J. Mol. Model*, 2011, **17**, 2501–2511.
31 A. D. Becke, *J. Chem. Phys.*, 1993, **98**, 5648–5652.
32 C. Lee, W. Yang and R. G. Parr, *Phys. Rev. B: Condens. Matter*, 1988, **37**, 785–789.
33 M. J. Frisch, G. W. Trucks, H. B. Schlegel, G. E. Scuseria, M. A. Robb, J. R. Cheeseman, J. A. Montgomery, T. Vreven Jr., K. N. Kudin, J. C. Burant, J. M. Millam, S. S. Iyengar, J. Tomasi, V. Barone, B. Mennucci, M. Cossi, G. Scalmani, N. Rega, G. A. Petersson, H. Nakatsuji, M. Hada, M. Ehara, K. Toyota, R. Fukuda, J. Hasegawa, M. Ishida, T. Nakajima, Y. Honda, O. Kitao, H. Nakai, M. Klene, X. Li, J. E. Knox, H. P. Hratchian, J. B. Cross, C. Adamo, J. Jaramillo, R. Gomperts, R. E. Stratmann, O. Yazyev, A. J. Austin, R. Cammi, C. Pomelli, J. W. Ochterski, P. Y. Ayala, K. Morokuma, G. A. Voth, P. Salvador, J. J. Dannenberg, G. Zakrzewski, S. Dapprich, A. D. Daniels, M. C. Strain, O. Farkas, D. K. Malick, A. D. Rabuck, K. Raghavachari, J. B. Foresman, J. V. Ortiz, Q. Cui, A. G. Baboul, S. Clifford, J. Cioslowski, B. B. Stefanov, G. Liu, A. Liashenko, P. Piskorz, I. Komaromi, R. L. Martin, D. J. Fox, T. Keith, M. A. Al-Laham, C. Y. Peng, A. Nanayakkara, M. Challacombe, P. M. W. Gill, B. Johnson, W. W. Chen, M. W. Gonzalez and J. A. C. Pople, *GAUSSIAN 03*, Gaussian, Inc, Wallingford CT, 2004.
34 T. A. Keith, *AIMAll*, TK Gristmill Software, Overland Park KS, USA, 2011.
35 The DA reaction of dimethylvinylborane (**2**) with isoprene can be used as a model for the reaction with myrcene. See ref. 9.
36 D. Cremer and E. Kraka, *Angew. Chem., Int. Ed. Engl.*, 1984, **23**, 627–628.
37 G. Merino, A. Vela and T. Heine, *Chem. Rev.*, 2005, **105**, 3812–3841.
38 E. Espinosa, I. Alkorta, J. Elguero and E. Molins, *J. Chem. Phys.*, 2002, **117**, 5529–5542.
39 C. F. Matta, A. A. Arabi and T. A. Keith, *J. Phys. Chem. A*, 2007, **111**, 8864–8872.
40 A. A. Arabi and C. F. Matta, *J. Phys. Chem. A*, 2009, **113**, 3360–3368.
41 J. L. López, A. M. Grana and R. A. Mosquera, *J. Phys. Chem. A*, 2009, **113**, 2652–2657.
42 M. M. Vallejos, E. L. Angelina and N. l. M. Peruchena, *J. Phys. Chem. A*, 2010, **114**, 2855–2863.

43 M. M. Vallejos and N. M. Peruchena, *J. Phys. Chem. A*, 2012, **116**, 4199.
44 F. Biegler-König, *J. Comput. Chem.*, 2000, **21**, 1040–1048.
45 L. R. Domingo and J. A. Saez, *Org. Biomol. Chem.*, 2009, **7**, 3576–3583.
46 L. R. Domingo, M. Arnó and J. Andrés, *J. Org. Chem.*, 1999, **64**, 5867–5875.
47 N. Grimblat and S. C. Pellegrinet, *Org. Biomol. Chem.*, 2013, **11**, 3733–3741.
48 R. F. W. Bader, T. T. Nguyen-Dang and Y. Tal, *Rep. Prog. Phys.*, 1981, **44**, 893–948.